Epitaxial ferromagnetic metal/GaAs(100) heterostructures

L. C. Chen,[a] J. W. Dong, B. D. Schultz, and C. J. Palmstrøm
Department of Chemical Engineering and Materials Science, University of Minnesota, Minneapolis, Minnesota 55455

J. Berezovsky, A. Isakovic, and P. A. Crowell
Department of Physics and Astronomy, University of Minnesota, Minneapolis, Minnesota 55455

N. Tabat
Recording Head Operations, Seagate Technology, Minneapolis, Minnesota 55435

(Received 6 April 2000; accepted 26 May 2000)

Ferromagnetic bcc-Fe_xCo_{1-x}(100) films have been successfully grown on GaAs(100) and $Sc_yEr_{1-y}As$(100) by molecular beam epitaxy. X-ray diffraction combined with reflection high energy electron diffraction and low energy electron diffraction patterns revealed the epitaxial orientation of bcc-Fe_xCo_{1-x}(100)$\langle 010\rangle \| GaAs(100)\langle 010\rangle$ and bcc-Fe_xCo_{1-x}(100) $\langle 010\rangle \| Sc_yEr_{1-y}As(100)\langle 010\rangle$. Rutherford backscattering channeling minimum yields, $\chi_{min} \sim 3\%$, suggest epitaxial films of high crystalline quality. Vibrating sample magnetometry measurements show in-plane uniaxial anisotropy and fourfold in-plane anisotropy for Fe_xCo_{1-x} grown on GaAs(100) and $Sc_yEr_{1-y}As$(100), respectively. The difference in magnetic anisotropy is interpreted as arising from the $Sc_yEr_{1-y}As$ interlayer altering the surface symmetry from twofold symmetry for GaAs(100) to fourfold symmetry. Misoriented substrates were also used to increase the step density in the [011] direction, which induced an additional uniaxial anisotropy with a [011] easy axis and a $[01\bar{1}]$ hard axis. This step structure symmetry-induced magnetic anisotropy generated a split field $\sim$50 Oe in the hard axis for bcc-Fe_xCo_{1-x}(100) grown on $Sc_yEr_{1-y}As$(100) surfaces. © *2000 American Vacuum Society.* [S0734-211X(00)07104-3]

I. INTRODUCTION

Ferromagnet/semiconductor heterostructures are of growing interest for the development of spintronic devices.[1] The electronic and magnetic properties of ferromagnets play an essential role in designing ferromagnet/semiconductor heterostructures for spin injection and spin tunneling injection. Ferromagnetic Fe_xCo_{1-x} alloys are technologically important because of their high permeability, saturation magnetization, and magnetocrystalline anisotropy combined with low coercivity.[2] In the bulk, the bcc-Fe_xCo_{1-x} lattice constant,[3] magnetic moment,[4] and easy axis[5] can be adjusted by changing the Fe to Co ratio. Although detailed studies of Fe/GaAs[6–8] and Fe_xCo_{1-x}/ZnSe[9,10] heterostructures have been performed, only recently have Fe_xCo_{1-x} films been grown on GaAs(100).[11,12] For epitaxial growth of elemental metallic films on GaAs, interfacial reactions generally occur. For Fe, the interfacial reactions result in As accumulation on the surface during growth.[13,14] The reactions can be minimized by low temperature growth and the use of an epitaxial diffusion barrier. $Sc_yEr_{1-y}As$ can be grown epitaxially on GaAs and is thermodynamically stable,[15] suggesting it may act as an excellent diffusion barrier between Fe_xCo_{1-x} and GaAs.

The GaAs(100) surface has twofold symmetry due to the sp^3 covalent bonding. The surface of $Sc_yEr_{1-y}As$(100), which has the NaCl crystal structure, is fourfold symmetric, and can be easily grown on GaAs(100).[15] Therefore, a $Sc_yEr_{1-y}As$ interlayer is expected to convert the surface symmetry from the twofold of GaAs(100) substrate to fourfold.

The substrate surface symmetry has been shown to control the in-plane magnetic anisotropy of ferromagnetic thin films grown on metallic substrates.[16] For GaAs(100), the surface steps run along the $\langle 011\rangle$ directions and are typically one bilayer high (2.83 Å).[17] The step density depends upon the misorientation of the surface with respect to the crystalline plane. Figure 1 shows the schematic drawing of GaAs(100) step structure with miscut $\theta°$ toward (111)A. The GaAs(100) substrate with a 4° miscut towards (111)A will have steps running along the $[01\bar{1}]$ direction with a terrace width $\sim$40 Å and density of $\sim 2.5\times 10^6$ steps/cm in the [011] direction (Fig. 1). This step structure will induce an additional twofold symmetry on the substrate surface.

In this article, the surface symmetry of the GaAs(100) substrate is altered by the use of a $Sc_yEr_{1-y}As$ interlayer and by the use of misorientated substrates. The effects on the magnetic properties of epitaxial Fe_xCo_{1-x} grown on these substrates will be discussed.

II. EXPERIMENTAL TECHNIQUES

n-doped GaAs(100) substrates [nominally 0°, 4°, 6°, 8°, and 10° miscut toward the (111)A surface] were indium bonded to molybdenum sample holders and loaded into the preparation chamber through a load lock of a modified VG Semicon V80H molecular beam epitaxy (MBE) system, which has a base pressure of $\sim 5\times 10^{-11}$ mbar. After outgas-

[a]Author to whom correspondence should be addressed; electronic mail: chenx102@umn.edu

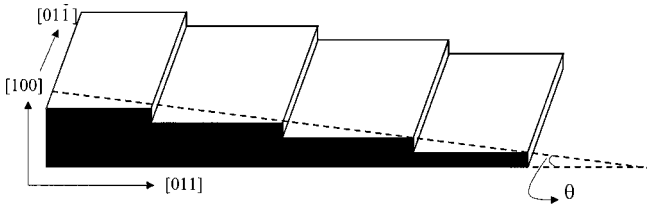

FIG. 1. Twofold surface symmetry of the GaAs(100) vicinal surface with $\theta°$ miscut towards (111)A.

sing at 250 °C in the preparation chamber, the samples were transported to the growth chamber where the depositions were performed. For each substrate, after native oxide removal at 610 °C under an As_4 flux, a 0.5 μm thick Si doped n ($10^{16}/cm^3$) GaAs buffer layer was grown at 585 °C. Each sample was cooled to 95 °C while maintaining the (2×4) surface reconstruction by controlling the valve opening of the arsenic valve cracker during the cooling procedure. For $Sc_yEr_{1-y}As$ interlayers, each sample was cooled to 350 °C under an As_4 flux, at which point 10 monolayers (~28 Å) of $Sc_yEr_{1-y}As$ were grown on the GaAs substrate using high temperature effusion cells for Sc and Er. Further cooling to 95 °C was performed without an As_4 flux. The Fe_xCo_{1-x} alloy films were grown at 95 °C by codeposition from an e-beam evaporation source for Fe and a high temperature effusion cell for Co. The samples were then rotated away from the effusion cells and cooled down to ~0 °C with the help of the liquid-nitrogen cooled cryo panel inside the MBE growth chamber. To protect the films from oxidation, the samples were capped by an ~20 Å Al protective layer deposited at ~0 °C prior to removal from the vacuum system. The alloy films were characterized *in situ* by reflection high energy electron diffraction (RHEED), low energy electron diffraction (LEED), and Auger electron spectroscopy (AES). *Ex situ* structural characterization included Rutherford backscattering spectrometry (RBS) and x-ray diffraction (XRD). The magnetic properties were characterized *ex situ* by vibrating sample magnetometry (VSM) and magneto-optical Kerr effect (MOKE) measurements. The MOKE setup was arranged such that both the longitudinal and transverse polarization could be measured.

III. RESULTS AND DISCUSSIONS

A. Growth and structure characterization

Figures 2 and 3 show the RHEED patterns of Fe_xCo_{1-x}/GaAs and $Fe_xCo_{1-x}/Sc_yEr_{1-y}As$/GaAs heterostructures, respectively. These RHEED patterns were obtained during growth. The RHEED patterns of Fe_xCo_{1-x} films exhibit well-defined Kikuchi lines, indicating high-quality single crystal growth of $Fe_xCo_{1-x}(100)$ on GaAs(100) and $Sc_yEr_{1-y}As(100)$. The spacing of RHEED streaks in the $\langle011\rangle$ and $\langle010\rangle$ directions showed a $\sqrt{2}$ ratio, indicating square surface unit cell, which was also observed by LEED. The RHEED patterns showed a $2\times$ reconstruction of Fe_xCo_{1-x} in both [011] and [$01\bar{1}$] directions which is similar to that observed for bcc-Fe/GaAs(100),[13]

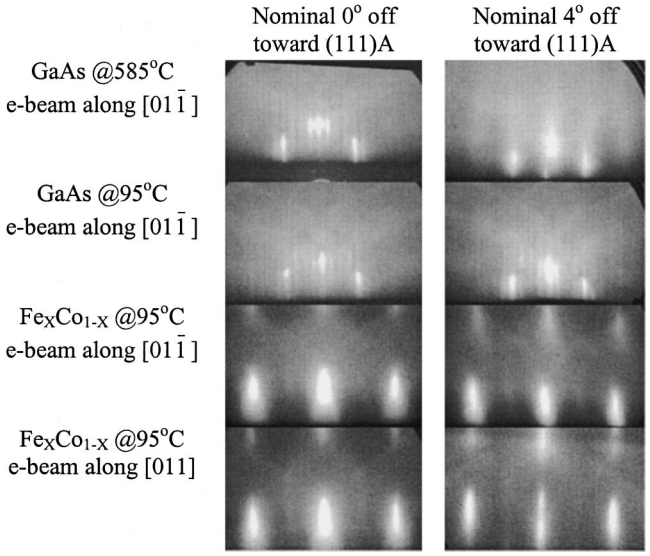

FIG. 2. Reflection high energy electron diffraction patterns of Fe_xCo_{1-x}/GaAs(100) heterostructures with 0° and 4° miscut toward (111)A.

bcc-Co/GaAs(100),[18] bcc-Co/ZnSe(100),[19] bcc-Fe/ZnSe(100),[19] and bcc-Fe_xCo_{1-x}/ZnSe(100).[9,10]

No detectable As, Ga, or other contaminants were detected by AES on ~200 Å thick Fe_xCo_{1-x} films grown directly on GaAs in contrast to the growth of Fe on sputter cleaned and annealed GaAs.[20] Figure 4 shows the XRD patterns of Fe_xCo_{1-x} grown on GaAs(100) and $Sc_yEr_{1-y}As(100)$. The XRD data combined with RHEED and LEED patterns reveal the epitaxial alignment of $Fe_xCo_{1-x}(100)\langle010\rangle\|GaAs(100)\langle010\rangle$ and $Fe_xCo_{1-x}(100)\langle010\rangle\|Sc_yEr_{1-y}As(100)\langle010\rangle\|GaAs(100)\langle010\rangle$. The out-of-plane lattice constants of Fe_xCo_{1-x} obtained from XRD are 2.856 Å in both cases, indicating an ~1% mismatch to

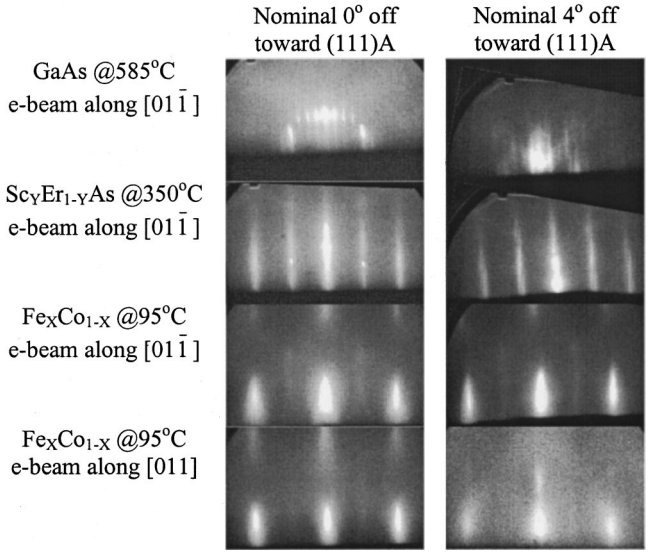

FIG. 3. Reflection high energy electron diffraction patterns of bcc $Fe_xCo_{1-x}(100)/Sc_yEr_{1-y}As(100)$/GaAs(100) heterostructures with 0° and 4° miscut toward (111)A.

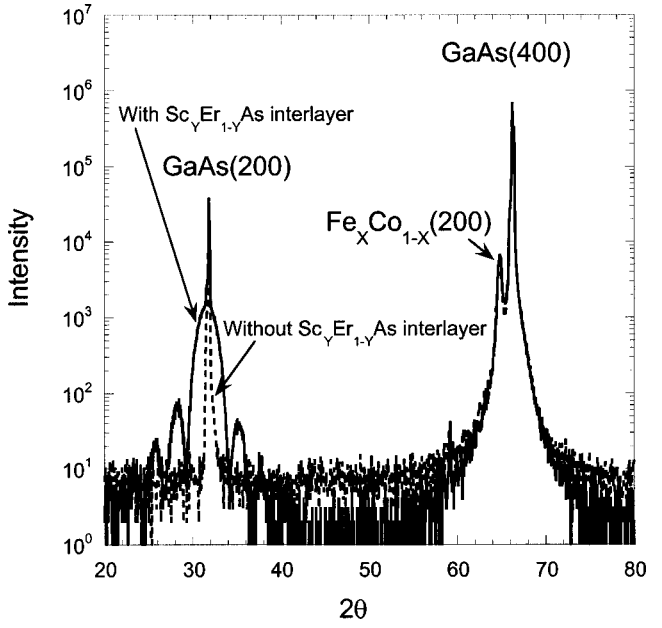

FIG. 4. X-ray diffraction patterns of Fe_xCo_{1-x} thin films grown on GaAs(100) substrates with and without $Sc_yEr_{1-y}As$ interlayer.

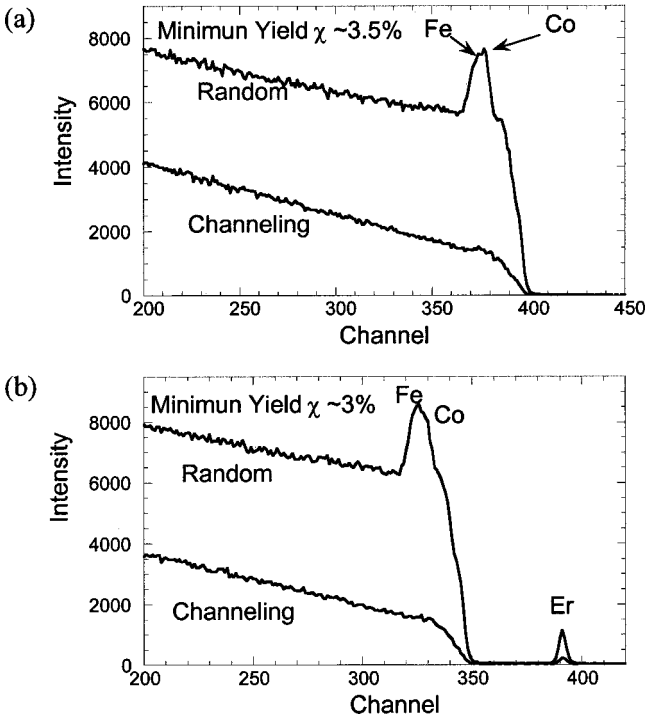

FIG. 5. RBS channeling and random spectra of (a) $Fe_xCo_{1-x}(100)$/GaAs(100)2×4 and (b) $Fe_xCo_{1-x}(100)/Sc_yEr_{1-y}As(100)/n$-GaAs(100).

half the unit cell of both $Sc_yEr_{1-y}As$ and GaAs. The out-of-plane lattice constants obtained from the XRD are close to the lattice constant of bulk bcc-$Fe_{0.5}Co_{0.5}$(2.85 Å),[21] suggesting that the Fe_xCo_{1-x} films are fully relaxed. In the case of Fe_xCo_{1-x} grown on $Sc_yEr_{1-y}As$, the XRD shows a set of satellite peaks around the GaAs(200) peak due to the finite thickness of the $Sc_yEr_{1-y}As$ layer. This indicates abrupt interfaces between Fe_xCo_{1-x}, $Sc_yEr_{1-y}As$, and GaAs.[22,23]

Figure 5 shows the RBS channeling and random spectra of $Fe_xCo_{1-x}(100)$/GaAs(100) and $Fe_xCo_{1-x}(100)/Sc_yEr_{1-y}As(100)$/GaAs(100). The minimum yield (χ_{min}) was obtained from the ratio of Fe_xCo_{1-x} peak area of channeling spectrum to that of random spectrum after background subtraction. The channeling minimum yields of $Fe_xCo_{1-x}(100)$/GaAs(100) and $Fe_xCo_{1-x}(100)/Sc_yEr_{1-y}As(100)$/GaAs(100) were 3.5% and 3%, respectively, which is indicative of high crystalline quality. The ~1:1 composition ratios of Fe_xCo_{1-x} were obtained from the deconvolution of RBS random spectra.

B. Magnetic characterization

VSM hysteresis loops with an applied magnetic field directed along the in-plane ⟨011⟩ and ⟨010⟩ crystalline azimuths for $Fe_xCo_{1-x}(100)/n$-GaAs(100) and $Fe_xCo_{1-x}(100)/Sc_yEr_{1-y}As(100)/n$-GaAs(100) are depicted in Figs. 6(a) and 6(b), respectively. The crystalline azimuths are referred to the GaAs substrate. In Fig. 6(a), it is obvious that the [011] and $[01\bar{1}]$ axes are different. A perfect square hysteresis loop was obtained when the applied field was directed in the [011] direction, suggesting this to be an easy axis. The hysteresis loops with the field along [010] and [001] were identical and are consistent with these being medium hard axes. The hysteresis loop obtained with the field along $[01\bar{1}]$ suggests this to be the hardest axis. This hard axis hysteresis loop has two symmetric split loops which are characterized by a split field (H_s).[24] The split field may result from the combination of magnetocrystalline anisotropy and uniaxial anisotropy.[25] This split field was found to be ~127 Oe.

It has been reported that the in-plane magnetic anisotropy of ferromagnetic metal/semiconductor heterostructures can be altered by surface morphology,[13,26] surface reconstruction,[6–9,13,19,27] and interfacial structures.[9,19,28–30] Since GaAs has a zincblende structure with sp^3 bonding, the bonding on the GaAs(100) surface tends to align in the [011] direction for As atoms or the $[01\bar{1}]$ direction for Ga atoms. Although the reason for the induced uniaxial anisotropy is not known, we believe that the uniaxial anisotropy results from the twofold surface symmetry of GaAs(100)[6–8] resulting from its sp^3 covalent bonding. This is in agreement with the STM studies of Fe grown on GaAs(100).[6–8]

Figure 6(b) shows the hysteresis loops of bcc-Fe_xCo_{1-x}(100) grown on $Sc_yEr_{1-y}As$(100). The VSM hysteresis loops in [011] and $[01\bar{1}]$ directions are identical, indicating the Fe_xCo_{1-x} films have fourfold anisotropy. Furthermore, the fourfold anisotropy results in no split field ($H_s=0$) in the $Fe_xCo_{1-x}/Sc_yEr_{1-y}As$/GaAs heterostructure. This suggests that the 127 Oe split field in the Fe_xCo_{1-x}/GaAs heterostructure results from the GaAs twofold surface symmetry. This implies that the interfacial structure dominates the magnetic anisotropy. It is unclear why the fourfold in-plane anisotropy of $Fe_xCo_{1-x}/Sc_yEr_{1-y}As$/

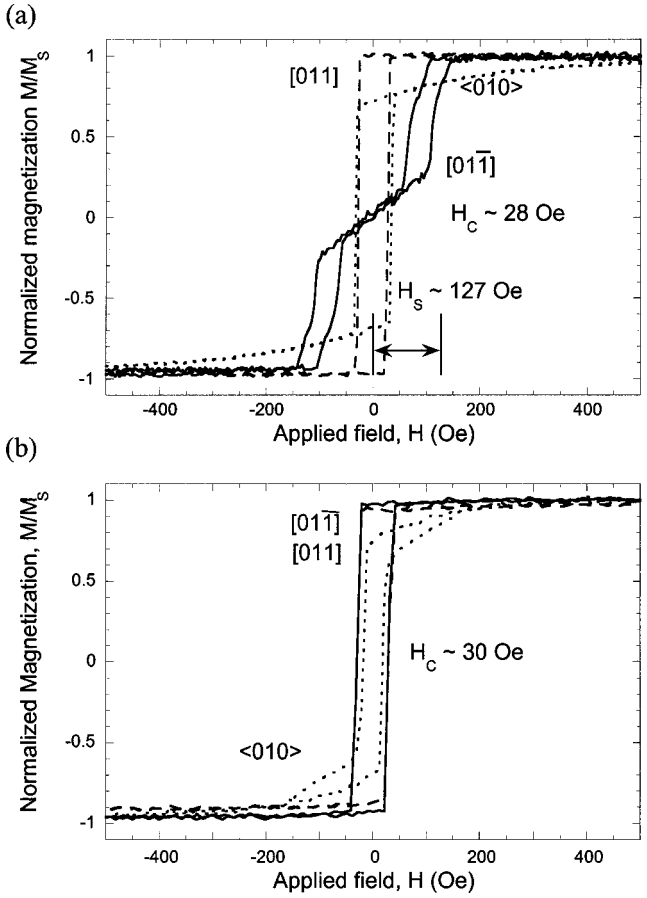

FIG. 6. VSM hysteresis loops of bcc-Fe_xCo_{1-x}(100) grown on GaAs(100) (a) without $Sc_yEr_{1-y}As$ and (b) with a $Sc_yEr_{1-y}As$ interlayer.

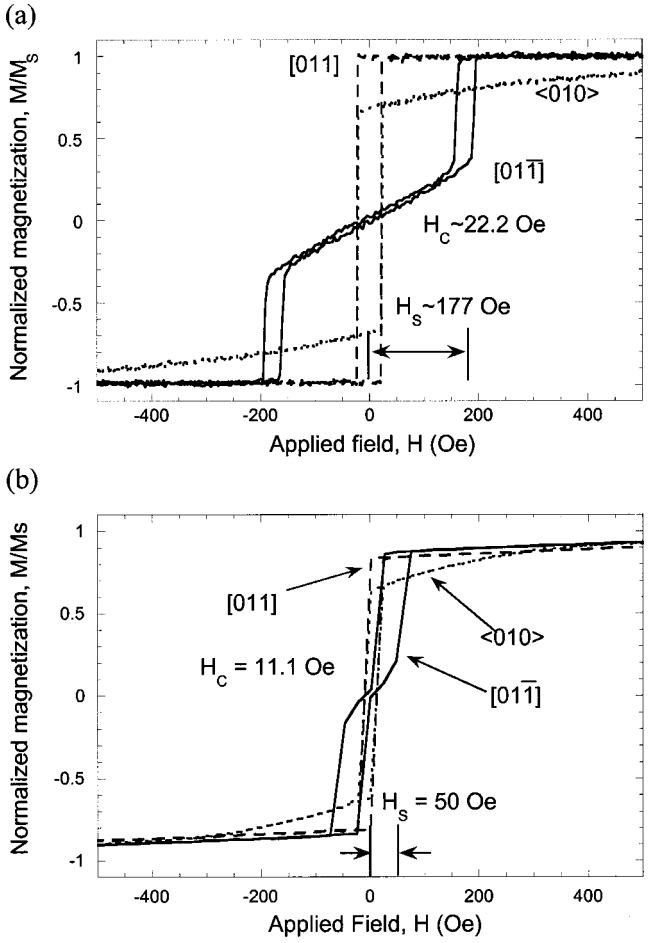

FIG. 7. VSM hysteresis loops of bcc-Fe_xCo_{1-x}(100) grown on GaAs(100) 4° miscut toward (111)A (a) without $Sc_yEr_{1-y}As$ and (b) with $Sc_yEr_{1-y}As$ interlayer.

GaAs(100) has two easy axes in the [011] and [01$\bar{1}$] directions instead of ⟨010⟩ or ⟨111⟩ easy axes as expected for bulk bcc-Fe_xCo_{1-x}.[31] This may result from the $Sc_yEr_{1-y}As$ crystal structure or from the combined effects of shape anisotropy and magnetocrystalline anisotropy.

Stepped surfaces can create symmetry-induced anisotropy in the elemental ferromagnetic thin films grown on the metallic substrates.[16,25,32] By using vicinal GaAs substrates, stepped surfaces can easily be formed. Figure 7(a) shows the hysteresis loops of Fe_xCo_{1-x} grown on GaAs(100) substrate with a 4° miscut toward (111)A. The [011], [01$\bar{1}$], and ⟨010⟩ are easy, hard, and medium hard axes, respectively. The hysteresis loops are similar to those obtained from Fe_xCo_{1-x} grown on GaAs(100) substrate without miscut except that the split field (H_s) increases from ~127 Oe without miscut to ~177 Oe with a 4° miscut in the hard axis. This 50 Oe increase in the split field results from the step symmetry-induced anisotropy. It is equivalent to applying a bias field in the easy axis direction.[24,33] Hence, the misoriented substrate makes the hard axis ([01$\bar{1}$]) require a larger field to saturate the magnetization. Figure 7(b) shows the hysteresis loops of Fe_xCo_{1-x} grown on GaAs(100) substrate with a 4° miscut toward (111)A and with a $Sc_yEr_{1-y}As$ interlayer. The hysteresis loops in the [011] and [01$\bar{1}$] are now different, indicating a uniaxial anisotropy. The easy axis is in the [011] direction and the hard axis is in the [01$\bar{1}$] direction. The hard axis has a set of split loops with ~50 Oe split field. Figure 8 shows the hard axis VSM hysteresis loops of bcc-Fe_xCo_{1-x}/$Sc_yEr_{1-y}As$/GaAs(100) and bcc-Fe_xCo_{1-x}/GaAs(100) with different miscut angles toward (111)A. It is obvious that the higher the misorientation angle, the larger the split field in both cases. The miscut angle dependence of the hard axis hysteresis loops suggests the higher miscut angle, the higher step density, and the stronger uniaxial anisotropy.

The crystal structure symmetry-induced magnetic anisotropy may be considered as an intrinsic anisotropy and the step structure symmetry-induced magnetic anisotropy as an extrinsic anisotropy. The intrinsic anisotropy cannot be changed without modifying the substrate crystal properties but the extrinsic anisotropy can be altered. The GaAs(100)(2×4) creates a uniaxial anisotropy with a [011] easy axis (intrinsic anisotropy) and the GaAs(100) miscut toward (111)A also creates a uniaxial anisotropy with [011] easy axis (extrinsic anisotropy). Therefore, this combination of intrinsic and extrinsic anisotropies induces in-plane magnetic anisotropy in the case of GaAs substrate (twofold crystalline surface symmetry). In the case of the $Sc_yEr_{1-y}As$

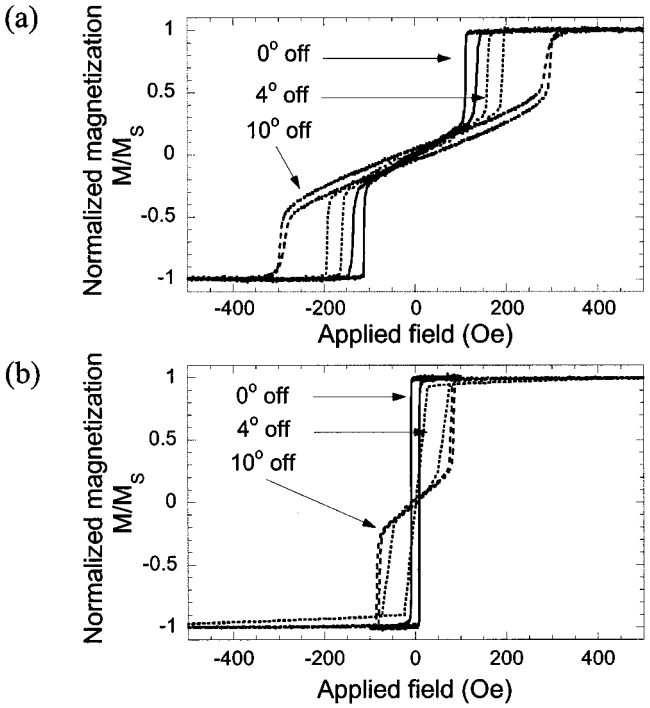

FIG. 8. Miscut angle dependence of VSM hard axis hysteresis loops for (a) bcc-Fe_xCo_{1-x}/*n*-GaAs(100) and (b) bcc-Fe_xCo_{1-x}/$Sc_yEr_{1-y}As$/*n*-GaAs(100) with 0°, 4°, and 10° miscut toward (111)A.

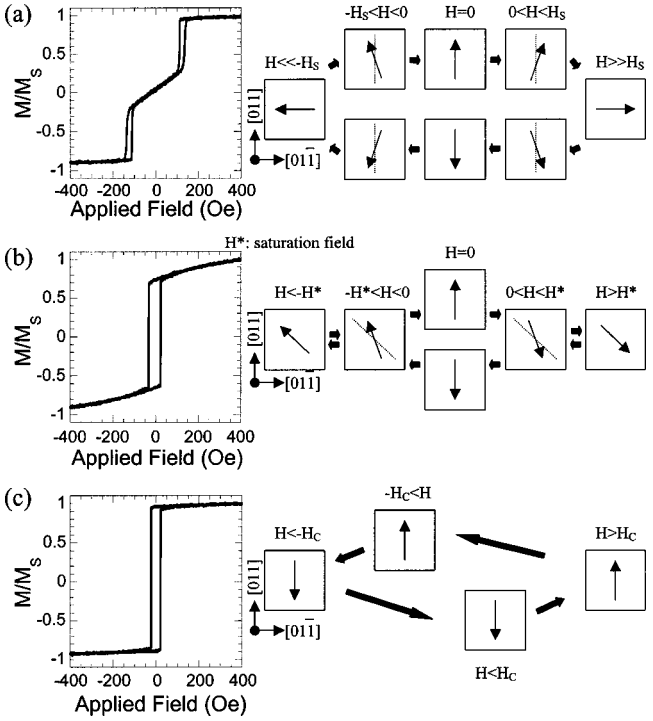

FIG. 10. Magnetic moments switching mechanism of bcc Fe_xCo_{1-x}(100)/GaAs(100). The applied field was directed along (a) $[01\bar{1}]$, the hard axis; (b) ⟨010⟩, the medium hard axes; and (c) [011], the easy axis.

(fourfold crystalline symmetry), the in-plane uniaxial anisotropy results exclusively from the extrinsic twofold surface symmetry.

Figure 9 shows the longitudinal and transverse MOKE spectra from a Fe_xCo_{1-x}/GaAs(100) without miscut. The external field was applied along the hard axis, the $[01\bar{1}]$ direction, and both the longitudinal (parallel to the applied field) and transverse (perpendicular to the applied field) in-plane magnetization were measured as the magnitude of the external field was varied. It is interesting to note that the in-plane magnetization perpendicular to the field increased dramatically when the applied magnetic field is reduced from its maximum values and reaches the split field. This suggests that the magnetic moments flip from being aligned parallel to the applied field and rotate nearly 90° from the hard axis ($[01\bar{1}]$) to the easy axis ([011]) when the uniaxial anisotropy dominates. As the applied field decreases, the linear relationship between in-plane longitudinal magnetization (parallel to the field) and applied field suggests a single domain coherent rotation. The in-plane magnetization perpendicular to the field remains almost the same, suggesting that the coherent rotation angle is too small to make a significant contribution to the longitudinal magnetization.

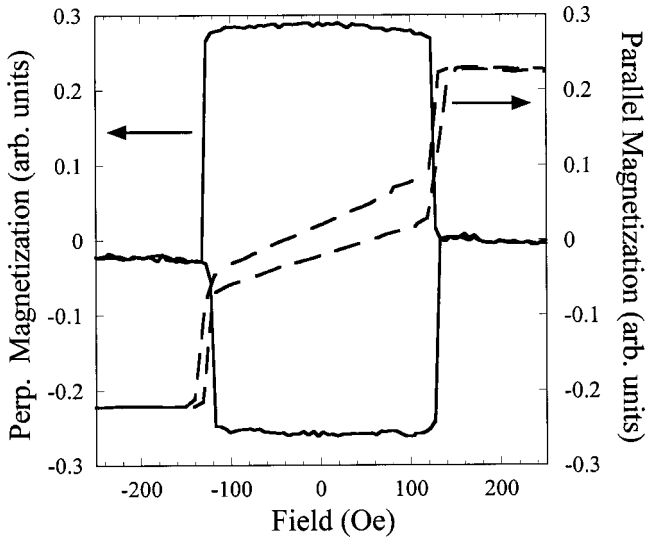

FIG. 9. Longitudinal and transverse magneto-optical Kerr effect (MOKE) spectrum of bcc-Fe_xCo_{1-x}(100)/GaAs(100)-2×4.

Figure 10 shows a possible magnetic moment switching mechanism. As discussed in the previous section, when the applied field is directed along the $[01\bar{1}]$ hard axis direction, the magnetic moments will be aligned under a saturation field; when the applied field is smaller than the split field ($-H_s<H$ or $H_s>H$), the magnetic moments rotate close to the [011] easy axis [as shown in Fig. 10(a)]. As the applied field is directed along the ⟨010⟩ directions [Fig. 10(b)], the magnetic moments will be aligned under a saturation field ($H>H^*$ or $H<-H^*$). The applied field can only partially align the magnetic moments toward the ⟨010⟩ direction and the magnetic moments rotate towards the easy axis (in [011] direction) when the applied field is decreased ($-H^*<H<-H_c$ or $H^*>H>H_c$). Hence, the magnetic moments will point to the [011] direction if there is no applied field. Therefore, the remanence in the ⟨010⟩ direction should be equal to

the projection of magnetic moments in the [011] direction to the ⟨010⟩ direction, which is cos 45° or 0.707. This is in an excellent agreement with the M_R/M_S ratio, which is ~0.7 in the ⟨010⟩ direction.

IV. CONCLUSIONS

Epitaxial single crystal bcc-Fe_xCo_{1-x}(100) thin films have been successfully grown on the GaAs(100) substrate. RHEED, LEED, and XRD data are consistent with the cube-on-cube crystal alignment of bcc-Fe_xCo_{1-x}(100) ⟨010⟩‖GaAs(100)⟨010⟩ and bcc-Fe_xCo_{1-x}(100) ⟨010⟩‖Sc_yEr_{1-y}As(100)⟨010⟩‖GaAs(100)⟨010⟩. The ~3% RBS minimum yields obtained from the channeling spectra indicate high quality single crystals. For the bcc-Fe_xCo_{1-x}(100)/GaAs(100) heterostructures, VSM hysteresis loops reveal a uniaxial magnetic anisotropy with [011] easy and $[01\bar{1}]$ hard axes. The uniaxial anisotropy was enhanced by increasing step density in the [011] direction. The uniaxial anisotropy can be eliminated by using a Sc_yEr_{1-y}As interlayer with fourfold symmetry. The intrinsic fourfold magnetic anisotropy of bcc-Fe_xCo_{1-x}(100)/Sc_yEr_{1-y}As(100)/GaAs(100) heterostructure can be made uniaxial by growth on vicinal substrates. In summary, we demonstrated the ability to control the magnetic anisotropy of ferromagnet/semiconductor by modifying the surface symmetries.

ACKNOWLEDGMENTS

This work was supported in part by Contract Nos. ONR-N/N00014-99-1-0233, DARPA/ONR-N/N00014-99-1-1005, NSF/DMR 981-9659, and by the Research Corporation (PAC).

[1]G. A. Prinz, Phys. Today **48**, 58 (1995).
[2]G. Y. Chin and J. H. Wernick, in *Ferromagnetic Materials*, edited by E. P. Wohlfarth (North-Holland, Amsterdam, 1980), Vol. 2, p. 55.
[3]K. Schwarz and D. R. Salahub, Phys. Rev. B **25**, 3427 (1982).
[4]T. R. McGuire, J. Appl. Phys. **40**, 1371 (1969).
[5]R. C. Hall, J. Appl. Phys. **31**, 157S (1960).
[6]E. M. Kneedler, P. M. Thibado, B. T. Jonker, B. R. Bennett, B. V. Shanabrook, R. J. Wagner, and L. J. Whitman, J. Vac. Sci. Technol. B **14**, 3193 (1996).
[7]E. M. Kneedler, B. T. Jonker, P. M. Thibado, R. J. Wagner, B. V. Shanabrook, and L. J. Whitman, Phys. Rev. B **56**, 8163 (1997).
[8]E. M. Kneedler and B. T. Jonker, J. Appl. Phys. **81**, 4463 (1997).
[9]C. J. Gutierrez, J. J. Krebs, and G. A. Prinz, Appl. Phys. Lett. **61**, 2476 (1992).
[10]C. J. Gutierrez, V. G. Harris, J. J. Krebs, W. T. Elam, and G. A. Prinz, J. Appl. Phys. **73**, 6763 (1993).
[11]L. C. Chen, J. W. Dong, B. D. Schultz, J. Berezovsky, P. A. Crowell, and C. J. Palmstrøm, presented at the 46th American Vacuum Society Meeting, Seattle, 1999.
[12]M. Dumm, M. Zölfl, R. Moosbühler, and G. Bayreuther, presented at the 44th Magnetism and Magnetic Materials Meeting, San Jose, 1999.
[13]J. J. Krebs, B. T. Jonker, and G. A. Prinz, J. Appl. Phys. **61**, 2596 (1987).
[14]J. R. Waldrop and R. W. Grant, Appl. Phys. Lett. **34**, 630 (1979).
[15]C. J. Palmstrøm and T. Sands, in *Contacts to Semiconductors*, edited by L. J. Brillson (Noyes, Park Ridge, NJ, 1993).
[16]R. K. Kawakami, E. J. Escorcia-Aparicio, and Z. Q. Qiu, Phys. Rev. Lett. **77**, 2570 (1996), and references therein.
[17]M. D. Pashley, K. W. Haberern, W. Friday, J. M. Woodall, and P. D. Kirchner, Phys. Rev. Lett. **60**, 2176 (1988).
[18]G. A. Prinz, Phys. Rev. Lett. **54**, 1051 (1985).
[19]B. T. Jonker, G. A. Prinz, and Y. U. Idzerda, J. Vac. Sci. Technol. B **9**, 2437 (1991).
[20]S. A. Chambers, F. Xu, H. W. Chen, I. M. Vitomirov, S. B. Anderson, and J. H. Weaver, Phys. Rev. B **34**, 6605 (1986).
[21]M. Shiga, in *Physics of Transition Metals—1980*, edited by P. Rhodes (Oxford, New York, 1980), p. 241.
[22]P. F. Miceli, C. J. Palmstrøm, and K. W. Moyers, Appl. Phys. Lett. **61**, 2060 (1992).
[23]P. F. Miceli and C. J. Palmstrøm, Phys. Rev. B **51**, 5506 (1995).
[24]W. Weber, C. H. Back, A. Bischof, Ch. Würsch, and R. Allenspach, Phys. Rev. Lett. **76**, 1940 (1996).
[25]H. P. Oepen, C. M. Schneider, D. S. Chuang, C. A. Ballentine, and R. C. O'Handley, J. Appl. Phys. **73**, 6186 (1993).
[26]M. Gester, C. Daboo, R. J. Hicken, S. J. Gray, A. Ercole, and J. A. C. Bland, J. Appl. Phys. **80**, 347 (1996).
[27]Y. B. Xu, E. T. M. Kernohan, D. J. Freeland, M. Tselepi, A. Ercole, and J. A. C. Bland, J. Magn. Magn. Mater. **198–199**, 703 (1999).
[28]A. Filipe, A. Schuhl, and P. Galtier, Appl. Phys. Lett. **70**, 129 (1997).
[29]A. Filipe and A. Schuhl, J. Appl. Phys. **81**, 4359 (1997).
[30]Y. B. Xu, E. T. Kernohan, M. Tselepi, J. A. C. Bland, and S. Holmes, Appl. Phys. Lett. **73**, 399 (1998).
[31]R. C. Hall, J. Appl. Phys. **31**, 157S (1960).
[32]A. Berger, U. Linke, and H. P. Oepen, Phys. Rev. Lett. **68**, 839 (1992).
[33]W. Weber, R. Allenspach, and A. Bischof, Appl. Phys. Lett. **70**, 520 (1997).